Published in final edited form as:
J Nucl Med. 2013 April ; 54(4): 549–555. doi:10.2967/jnumed.112.111542.

Improved Accuracy of Myocardial Perfusion SPECT for the Detection of Coronary Artery Disease by Utilizing a Support Vector Machines Algorithm

Reza Arsanjani[1], **Yuan Xu**[1], **Damini Dey**[2,3], **Matthews Fish**[4], **Sharmila Dorbala**[5], **Sean Hayes**[1], **Daniel Berman**[1,3], **Guido Germano**[1,3], and **Piotr Slomka**[1,3]

[1]Departments of Imaging and Medicine, and Cedars-Sinai Heart Institute, Cedars-Sinai Medical Center, Los Angeles, CA

[2]Biomedical Imaging Research Institute, Department of Biomedical Sciences, Cedars-Sinai Medical Center, Los Angeles, CA

[3]David Geffen School of Medicine, University of California Los Angeles, Los Angeles, CA

[4]Oregon Heart and Vascular Institute, Sacred Heart Medical Center, Springfield, OR

[5]Brigham and Women's Hospital, Boston, MA

Abstract

We aimed to improve the diagnostic accuracy of automatic myocardial perfusion SPECT (MPS) interpretation analysis for prediction of coronary artery disease (CAD) by integrating several quantitative perfusion and functional variables for non-corrected (NC) data by support vector machines (SVM), a computer method for machine learning.

Methods—957 rest/stress ^{99m}technetium gated MPS NC studies from 623 consecutive patients with correlating invasive coronary angiography and 334 with low likelihood of CAD (LLK < 5%) were assessed. Patients with stenosis ≥ 50% in left main or ≥ 70% in all other vessels were considered abnormal. Total perfusion deficit (TPD) was computed automatically. In addition, ischemic changes (ISCH) and ejection fraction changes (EFC) between stress and rest were derived by quantitative software. The SVM was trained using a group of 125 pts (25 LLK, 25 0-, 25 1-, 25 2- and 25 3-vessel CAD) using above quantitative variables and second order polynomial fitting. The remaining patients (N = 832) were categorized based on probability estimates, with CAD defined as (probability estimate ≥ 0.50). The diagnostic accuracy of SVM was also compared to visual segmental scoring by two experienced readers.

Results—Sensitivity of SVM (84%) was significantly better than ISCH (75%, $p < 0.05$) and EFC (31%, $p < 0.05$). Specificity of SVM (88%) was significantly better than that of TPD (78%, $p < 0.05$) and EFC (77%, $p < 0.05$). Diagnostic accuracy of SVM (86%) was significantly better than TPD (81%), ISCH (81%), or EFC (46%) ($p < 0.05$ for all). The Receiver-operator-characteristic area-under-the-curve (ROC-AUC) for SVM (0.92) was significantly better than TPD (0.90), ISCH (0.87), and EFC (0.60) ($p < 0.001$ for all). Diagnostic accuracy of SVM was comparable to the overall accuracy of both visual readers (85% vs. 84%, $p < 0.05$). ROC-AUC for SVM (0.92) was significantly better than that of both visual readers (0.87 and 0.88, $p < 0.03$).

Corresponding Author Info: Piotr J. Slomka, PhD, Artificial Intelligence in Medicine Program, 8700 Beverly Blvd, Ste A047N, Los Angeles, CA 90048, USA, Ph: 310-423-4348, piotr.slomka@cshs.org.
First Author Info: Reza Arsanjani, MD (Post-doctoral fellow), Cedars-Sinai Medical Center, 8700 Beverly Blvd, Taper A238, Los Angeles, CA 90048, USA, Ph: 310-423-4332, Reza.Arsanjani@cshs.org

Conclusion—Computational integration of quantitative perfusion and functional variables by SVM approach allows significant improvement of diagnostic accuracy of MPS, and can significantly outperform visual assessment based on ROC analysis.

Keywords

Automated Quantification; Coronary Artery Disease; Myocardial Perfusion SPECT; Total Perfusion Deficit; Support Vector Machines; Machine Learning

Coronary artery disease (CAD) is the leading cause of morbidity and mortality worldwide (1,2). Myocardial perfusion SPECT (MPS) is the most commonly used noninvasive stress imaging modality for diagnosis of CAD (3). Multiple MPS features including quantitative perfusion and functional variables have been previously used for diagnosis of obstructive CAD (4–8) and they are reported routinely by nuclear cardiology software. However, algorithms for combining and integrating these variables to improve the overall test accuracy have not been well developed. Currently none of the software tools provides combined diagnostic score based on multiple quantitative features.

Support Vector Machines (SVM), a kernel-based method (9) is a machine learning algorithm. It has been applied in various fields including computational biology due to its high overall accuracy, ability to deal with large datasets, and its flexibility in modeling diverse sources of data (10). SVM is a classifier, where a set of input data with several features are used to assign objects to multiple categories (10). SVM uses the concept of margin maximization (distances between hyper-surfaces defined in multi-dimensional variable space) to discriminate between two categories. Margins are computed by various kernel functions, which allow the SVM to classify with nonlinear class boundaries by transforming the input variables via nonlinear mappings. Furthermore, in certain implementations it is also possible to obtain probability estimates for particular classification (11).

In the current study, we aimed to investigate whether integrating quantitative perfusion and functional MPS variables using a SVM statistical learning algorithm demonstrate an improvement in the diagnostic accuracy of automated analysis in predicting severe stenosis, using invasive coronary angiography as the gold standard. To our knowledge, such an approach has not been previously reported for quantitative MPS. Such a tool may easily be integrated within currently available quantitative nuclear cardiology software programs in order to provide improved automated diagnostic score for interpretation of MPS results.

MATERIALS AND METHODS

Patients Population

Consecutive subjects who were referred to the Nuclear Medicine Department of Sacred Heart Medical Center, Eugene, Oregon, from March 1, 2003 to December 31, 2006 for rest and stress electrocardiography (ECG)-gated MPS, in whom gated information was available for both phases, were selected (12). All patients with a prior history of CAD or significant valve disease were excluded. MPS and coronary angiography had to be performed within 60 days without a significant intervening event. The low likelihood (LLk) studies were obtained from patients who performed an adequate treadmill stress test, did not have correlating coronary angiography available, but had < 5% likelihood of CAD using the Diamond and Forrester criteria based on age, sex, symptoms, and ECG response to adequate treadmill stress testing (13). Based on these selection criteria, 957 sequential studies were identified to form the study group.

Training and Testing Groups

This population consisted of two subgroups of patients: 623 patients with correlative angiography as described above and 334 patients with a LLk of CAD who were classified as normal. We chose to split our population into minimal training and larger testing groups in order to keep the testing population as large as possible. From our internal experience in perfusion quantification with normal databases, a small number of LLk datasets (25–50) were sufficient for the creation of normal databases (14), while increasing that number did not significantly change the normal distribution. In this application, we needed to include a representative population with varying degree of the disease. We chose to include an equal number of cases assigned to normal and abnormal groups in order to ensure equal contribution from different perfusion and/or functional abnormalities. The objective was to create a balanced model that would be applicable to normal and abnormal scans. Therefore, the training group consisted of 125 patients (25 LLK, 25 0-vessel, 25 1-vessel, 25 2-vessel, and 25 3-vessel CAD). The remaining 832 patients were used during the testing phase. The clinical characteristics of the two groups are listed in Table 1. The study protocol was approved by the Institutional Review Board (IRB).

Image Acquisition and Reconstruction Protocols

The details of image acquisition and tomographic reconstruction have been previously described (15). In brief, studies were performed by using standard ^{99m}Tc-sestamibi rest/stress protocols. All subjects were imaged at 60 min after the administration of ^{99m}Tc-sestamibi at rest followed by stress images taken at 15–45 min after either radiopharmaceutical injection during treadmill testing or adenosine infusion with low-level exercise. Vertex, dual-detector scintillation cameras (Philips Medical Systems, Milpitas, CA, USA) with low energy, high-resolution collimators were used to acquire MPS.

Ungated and gated tomographic reconstruction was performed by use of the AutoSPECT (16) and Vantage Pro programs (Philips Medical Systems). Emission images were automatically corrected for non-uniformity, radioactive decay, and motion during acquisition, and subjected to three-point spatial smoothing. Attenuation-correction was not used in this study. The alignment of the projection data to the reconstruction matrix was applied to determine the mechanical center of rotation. Butterworth filters were applied to obtain the MPS with an order of 10 and cutoff of 0.50 for rest MPS, and an order of 5 and cutoff of 0.66 for stress MPS. For gated images time binning was performed both into 8-bin (70%) and 16-bin (30%).

Automated Analysis

In this proof-of-concept study, we have selected three common quantitative features routinely used during interpretation of MPS (two perfusion and one functional feature) to provide a minimal set of quantitative variables known to be clinically important, and conservatively guarding against any potential over-fitting with a larger number of features.

Stress Total Perfusion Deficit (TPD)—Stress MPS images were quantified using normal limits and previously developed simplified approach (6). Perfusion parameters were derived automatically based on the concept of total perfusion deficit (TPD) (17). Briefly, an ellipsoidal model and contours derived by the QPS algorithm (18–20) were used to extract polar map samples. An optimal normalization factor was established by an iterative search for the minimal absolute count difference between the counts in the normal part of the myocardium and the corresponding count distribution in the normal database. This scheme avoided normalization based on an arbitrary selection of pixels (maximum or percentile maximum). Subsequently, an abnormality threshold of 3.0 average (mean absolute) deviations was applied, which is approximately equivalent to 2.5 SD, to estimate the extent

of hypoperfusion. This value is similar to the threshold used in other MPS quantification methods (21). The perfusion defect extent was calculated as the percentage of the total surface area of the left ventricle for which test data were below the abnormality threshold.

Ischemic Changes (ISCH)—Following image registration and normalization as previously described (5), the stress–rest count difference was derived from the voxels contained within only the stress contour volume, since rest scans were spatially aligned to stress scans. The integrated count differences were then divided by the total rest counts, resulting in a relative count change measure, which we defined as the measure of ischemia (ISCH). This perfusion measurement does not require normal databases and is obtained independently from the TPD measurement. This measure has a complementary character to TPD measurement.

Post-stress Ejection Fraction Changes (EFC)—EFC changes have been shown to be helpful in diagnosing CAD (8). However, an exact combination of EFC with perfusion measurements in diagnosing CAD has not been established. Stress and rest left ventricular (LV) ejection fraction (EF) were automatically calculated using Quantitative Gated SPECT (QGS) utilizing gated perfusion images via a volume-based approach as previously described (22). The LV cavity volume was measured as the territory bound by the endocardium and its valve plane for every interval in the cardiac cycle. The end-diastolic (EDV) and end-systolic (ESV) volumes were identified using the time-volume curve (22). The differences between stress and rest EF was defined as EFC.

Motion and Thickening Changes (MTC)—Automated regional motion and thickening scores were derived as previously described by our group (23). Regional motion in millimeters (mm) was defined as the distance between end-diastolic (ED) and end-systolic (ES) mid-myocardial surface in the direction normal to the mid-myocardial surface for each polar map location. Thickening at each polar map point in % was defined as the increase of myocardial thickness (distance between the endocardial and epicardial surface) at the ES phase as compared to the ED phase, and also in the direction of the mid-myocardial surface normal (23). Using normal motion and thickening limits created based on LLk patients, automated motion and thickening scores were derived using a 17-segment model (23). The motion score ranged between 0 to 5: 0 normal, 1 mildly, 2 moderately, 3 severely hypokinetic, 4 akinetic, and 5 dyskinetic. The thickening score ranging between 0 to 3: 0 normal, 1 mildly abnormal, 2 moderately to severely abnormal, and 3 no systolic wall thickening (23). The motion and thickening change scores were calculated separately by subtracting the rest image score from the stress image score.

Visual Analysis

Visual interpretation of MPS images was based on short axis, horizontal, and vertical long-axis tomograms divided into 17 segments using QPS interactive 17-segment graph (22). MPS images were scored independently by two expert board-certified readers (Reader 1 with 30 years and Reader 2 with more than 10 years of clinical experience in nuclear cardiology) using a five-point scoring system (0, normal; 1, mildly decreased; 2, moderately decreased; 3, severely decreased; and 4, absence of segmental uptake). Visual reading was performed with the expert being blinded to computer-generated myocardial perfusion quantification results or any clinical information, such as patient history. The readers scored both the stress and rest 17 perfusion segments using the 5-point scale described above. The readers could review stress and rest perfusion data, raw projection data and gated function data (24). Subsequently, summed stress scores (SSS) and summed rest scores (SRS) were calculated by summing the 17 segment stress and rest scores, respectively. In addition, a summed difference score (SDS) was calculated as SSS minus SRS. All visual scores were

recorded automatically in the batch files and directly converted for the statistical analysis, eliminating manual transfer.

Support Vector Machines Algorithm

Model creation—We used SVM statistical learning algorithm, open source LIBSVM implementation (11), to combine quantitative perfusion (TPD and ISCH) and functional variables (EFC). In addition, we also combined quantitative perfusion (TPD and ISCH) with functional variables MTC and absolute stress EDV and ESV. The SVM algorithm has been extensively described in computer science literature (25,26). Briefly, SVM searches for the optimal division of the feature space (to normal/abnormal) with a hyper-plane by maximizing margins (distances) from the plane to support vectors (points closest to the plane). The points positioned clearly outside of the hyper-plane on two sides were discarded by the algorithm when searching for the hyperplane. This method is resistant to over-fitting, as only the points close to hyper-plane (decision plane) are considered in the fitting. The distances from the hyper-plane are then converted to probability estimates, which provide an estimate of probability of the outcome category, as described in LIBSVM: A library for support vector machines by Chang and colleagues (11).

In SVM, the training vectors (x_i) are mapped into a n-dimensional feature space by the kernel functions. Kernel functions other than linear allow non-linear class boundaries. Mathematically, any kernel function is defined by

$$K(x_i, x_j)=\Phi(x_i)^T\Phi(x_j)(11) \quad (1)$$

Where x_i are the training vectors. There are four basic kernels available on SVM: linear, polynomial, radial, and sigmoid (27). We used a polynomial kernel of degree (d =2) in the form of equation 2 (11):

$$K(x_i, x_j)=(y^*x_i, x_j)^d \quad (2)$$

to allow nonlinear classification. SVM transforms the nonlinear feature space to higher-dimensional linear space with the use of the kernel function. The penalty for the positive class was assumed to be equal to the ratio of abnormal to normal cases (1.5 in the training set), as recommended for unbalanced datasets (27). Subsequently, optimal parameters for the penalty factor for the error term (C) and kernel parameter γ, were found by a grid search technique, where the combination of C and γ are optimized for the best cross-validation accuracy (27). The grid search analysis is performed only on the training set. Based on these parameters, the SVM model was created.

Furthermore, for comparison we assessed the diagnostic accuracy of the SVM model using linear kernel function, with d equal to 1 in equation 2.

Testing—The test group patients (N = 832) were divided by SVM into 2 categories (CAD, and no CAD) in the testing phase. The model defined as described above was validated with the test group. None of the cases used in the model creation used in the testing phase. The probability estimates returned by SVM were categorized as normal (< 0.50) and abnormal (≥0.50). These probability estimates were used to construct ROC curves.

Definition of Abnormal MPS

Automated Analysis—SVM threshold was derived automatically during the testing phase. In order to compare diagnostic performance of the SVM method to individual features, we used previously established thresholds. A TPD value of ≥ 3% on per-patient

basis was considered abnormal (12). The ISCH value of ≥ 3% was considered abnormal based on previously established thresholds (5). An EFC value of ≥ 5% was considered abnormal based on previously established thresholds (8).

Visual Analysis—SSS ≥ 4 was considered abnormal (12). SDS ≥ 2 was considered abnormal (12).

Conventional Coronary Angiography

Conventional coronary angiography was performed according to standard clinical protocols within 60 days of the myocardial perfusion examination. All coronary angiograms were visually interpreted by an experienced cardiologist. A stenosis of 50% or greater narrowing of luminal diameter of the left main or 70% or greater narrowing of the other coronary arteries was considered significant and was used as the gold standard for the detection of CAD.

Statistical Analysis

Continuous variables were expressed as the means ± standard deviation, and categorical variables were expressed as percentages (%). A Z-test was performed to compare the sensitivity, specificity, and accuracy of the various quantitative variables versus SVM, as well as SVM versus visual analysis. For all analyses, p values < 0.05 were considered statistically significant. Receiver-operator-characteristic (ROC) curves were analyzed to evaluate the ability of SVM versus various quantitative variables for forecasting ≥70% stenoses of the coronary arteries. In addition, ROC curves were also analyzed to evaluate the ability of SVM classification versus visual scoring for forecasting ≥70% stenoses of coronary artery. The differences between the ROC areas under the curves (ROC-AUC) were compared using the Delong method (28).

RESULTS

SVM versus Quantitative Perfusion and Functional Analysis

Figure 1 compares the sensitivity, specificity, and accuracy of the quantitative measures TPD, ISCH, EFC, and SVM for detection of ≥ 70% CAD on a per-patient basis. When the TPD was compared to the SVM analysis, the specificity and accuracy of SVM was significantly higher than the TPD analysis ($p < 0.05$). The sensitivity, however, was similar between the SVM (84%) and TPD (85%) analysis. When ISCH was compared to the SVM analysis, the sensitivity and accuracy of SVM was significantly higher than that for TPD ($p < 0.05$). The specificity, however, was similar between the SVM and ISCH analysis. The sensitivity, specificity, and accuracy of SVM were higher than EFC ($p < 0.05$). The ROC curves comparing TPD, ISCH, EFC, and SVM probability estimates are shown in Figure 2. Table 2 also demonstrates the number of patients in whom the diagnosis was correctly changed based using SVM versus TPD alone. In the majority of cases, one or both of the other factors (ISCH and EFC) established the correct diagnosis. The ROC-AUC for SVM probability estimates (0.92) was significantly better ($p < 0.001$ for all) versus TPD (0.90), ISCH (0.87), and EFC (0.60).

The sensitivity, specificity, and diagnostic accuracy of SVM using linear kernel function (d=1) for detection of > 70% CAD on per-patient basis. The sensitivity was 89%, the specificity was 77%, and the overall diagnostic accuracy was 82%. When comparing polynomial SVM to linear SVM, the diagnostic accuracy and specificity were significantly higher ($p < 0.05$), while the sensitivity was significantly lower ($p = 0.046$).

We also assessed the sensitivity, specificity, and diagnostic accuracy of SVM by combining quantitative perfusion (TPD and ISCH) and functional variables regional MTC and absolute stress EDV and ESV, which are shown in Table 3. The sensitivity of quantitative perfusion with MTC and absolute volumes significantly decreased, while the specificity significantly improved when compared to the combined method using quantitative and changes in EF, with accuracy remaining approximately the same. In addition, the ROC-AUC was also not significantly different.

SVM versus Visual Analysis

Figure 3 compares the sensitivity, specificity, and accuracy of SVM versus to readers (SSS) for detection of ≥ 70% CAD on per-patient basis. The sensitivity, specificity, and accuracy of SVM were comparable to Reader 1. When compared to Reader 2, the sensitivity of SVM was significantly better ($p < 0.05$). The specificity and diagnostic accuracy of SVM were similar to Reader 2. The ROC curves comparing SVM and the two visual readers are shown in Figure 4. The ROC-AUC for SVM probability estimates was significantly better ($p < 0.03$) than both readers. In addition, we also compared the sensitivity, specificity, and accuracy of SVM versus SDS in Figure 3 for detection of ≥ 70% CAD on per-patient basis. These values were not significantly different than those obtained using SSS.

DISCUSSION

In this study, we were able to demonstrate significant improvement in diagnostic accuracy for detection of obstructive CAD utilizing the SVM machine learning algorithm, which combined quantitative perfusion and functional variables. There has been significant interest in improving the overall diagnostic performance on MPS, in hopes of identifying individuals with significant CAD who might benefit from earlier intervention, as well as preventing the need for unnecessary invasive evaluation in patients with false positive MPS (21). Although individual quantitative measurements have previously been used for diagnosis of obstructive CAD (5,8,15), to our knowledge, this is the first study indicating improvement in diagnostic accuracy of MPS utilizing learning algorithms combining multiple features.

Statistical learning algorithms have been used in cardiovascular medicine to predict multiple features including those at increased risk of decompensated heart failure (29) as well as predictors of onset of atrial fibrillation (30). Prior studies have demonstrated that quantitative analysis can be a useful supplement to the visual analysis (31,32), providing an accurate and objective method for assessment of the extent, severity, and reversibility of perfusion defects. The ability to combine multiple quantitative features could further enhance the value of quantitative MPS tools for diagnosis of obstructive CAD. In this study, we have demonstrated that the combination of SVM with the currently available automated software improves significantly the overall diagnostic accuracy of the quantitative analysis system. To our knowledge, this is the first report of SVM application for this purpose.

We also compared the diagnostic accuracy of SVM using different quantitative perfusion and functional analysis. The combination of quantitative perfusion and regional MTC using SVM resulted in a significant decline in sensitivity, significant improvement in specificity, and similar accuracy. These findings are consistent with prior studies demonstrating a decline in sensitivity and improvement in specificity when using regional functional data (33). Therefore, it appears that both changes in global and regional wall motion between stress and rest provide incremental diagnostic value when utilizing the SVM combined method; however, global ejection fraction may be a more reasonable approach based on the fact that both specificity and accuracy improve without a significant decline in sensitivity.

We compared the diagnostic accuracy of SVM versus two experienced visual readers. Prior studies have shown less variability when using automated analysis versus semi-quantitative analysis (34), especially when compared to less experienced readers (35,36). The diagnostic accuracy of SVM, combining multiple quantitative features, was at least comparable to two experienced readers from high volume centers. Therefore, SVM analysis might play an integral role as an automated diagnostic tool suggesting diagnostic classification (and potentially the decision value to indicate the confidence in decision) for the less experienced reader who may be less certain about normal variation in uptake (37). The SVM library could be easily integrated with standard quantitative nuclear cardiology tools (SVM library is freely available and can be distributed with other software). SVM probability estimates have a simple intuitive interpretation as the distance from the decision line, which can facilitate clinical acceptance and allow a measure of the confidence in the proposed classification.

This study has several limitations. Coronary angiography was used as the gold standard for this study with its known limitations. The degree of stenosis was interpreted visually rather than quantified, which may have resulted in overestimation of stenosis. In addition, patients with LLk of CAD were included in our analysis and were considered to have a normal angiogram. Furthermore, integration using SVM was applied to a population with suspected but not known CAD. However, the detection of CAD is typically useful only in this group. In the current study, we excluded patients with a prior history of CAD and significant valve disease, therefore the results of this study might not be applicable to these patients. We selected only a limited number of quantitative features in order to demonstrate proof-of-concept and prevent over-fitting in large feature space. However, even with such a limited number of features, we could demonstrate significant improvement in diagnostic accuracy. In addition, we used a binary approach (normal versus abnormal) both for visual and automatic analysis. Further studies are likely needed to define the possible equivocal range and the potential use of such a category in the context of disease detection. Furthermore, although the splitting of training and testing was consistent with our internal experience, future studies using different training arrangements may be needed to further evaluate this proof-of-concept. Finally, although we had a large patient population, the results were obtained on only one particular camera system. Based on these limitations, further multicenter evaluations will be required to confirm these results.

CONCLUSION

Computational integration of several quantitative perfusion and functional variables by SVM approach allows improvement of diagnostic accuracy and specificity of MPS. In addition, the diagnostic accuracy of SVM was at least comparable to visual analysis, and can potentially outperform visual assessment based on ROC analysis.

Acknowledgments

This research was supported in part by grants R01HL089765 from the National Heart, Lung, and Blood Institute/ National Institutes of Health (NHLBI/NIH). Its contents are solely the responsibility of the authors and do not necessarily represent the official views of the NHLBI. Cedars-Sinai Medical Center receives royalties for the quantitative assessment of function, perfusion, and viability, a portion of which is distributed to some of the authors of this manuscript (DB, GG, PS). We would like to thank Caroline Kilian and Arpine Oganyan for editing and proof-reading the text.

REFERENCES

1. Yusuf S, Reddy S, Ounpuu S, et al. Global burden of cardiovascular diseases: part I: general considerations, the epidemiologic transition, risk factors, and impact of urbanization. Circulation. 2001; 104:2746–2753. [PubMed: 11723030]

2. Yusuf S, Reddy S, Ounpuu S, et al. Global burden of cardiovascular diseases: Part II: variations in cardiovascular disease by specific ethnic groups and geographic regions and prevention strategies. Circulation. 2001; 104:2855–2864. [PubMed: 11733407]
3. Sharir T, Ben-Haim S, Merzon K, et al. High-speed myocardial perfusion imaging initial clinical comparison with conventional dual detector anger camera imaging. JACC Cardiovasc Imaging. 2008; 1:156–163. [PubMed: 19356422]
4. Amanullah AM, Berman DS, Hachamovitch R, et al. Identification of severe or extensive coronary artery disease in women by adenosine technetium-99m sestamibi SPECT. Am J Cardiol. 1997; 80:132–137. [PubMed: 9230147]
5. Slomka PJ, Nishina H, Berman DS, et al. Automatic quantification of myocardial perfusion stress-rest change: a new measure of ischemia. J Nucl Med. 2004; 45:183–191. [PubMed: 14960634]
6. Slomka PJ, Nishina H, Berman DS, et al. Automated quantification of myocardial perfusion SPECT using simplified normal limits. J Nucl Cardiol. 2005; 12:66–77. [PubMed: 15682367]
7. Abidov A, Bax JJ, Hayes SW, et al. Transient ischemic dilation ratio of the left ventricle is a significant predictor of future cardiac events in patients with otherwise normal myocardial perfusion SPECT. J Am Coll Cardiol. 2003; 42:1818–1825. [PubMed: 14642694]
8. Johnson LL, Verdesca SA, Aude WY, et al. Postischemic stunning can affect left ventricular ejection fraction and regional wall motion on post-stress gated sestamibi tomograms. J Am Coll Cardiol. 1997; 30:1641–1648. [PubMed: 9385888]
9. Cortes C, Vapnik V. Support-vector networks. Machine Learning. 1995; 20:273–297.
10. Ben-Hur A, Ong CS, Sonnenburg S, et al. Support vector machines and kernels for computational biology. PLoS Comput Biol. 2008; 4:e1000173. [PubMed: 18974822]
11. Chang C-C, Lin C-J. LIBSVM: A library for support vector machines. ACM Trans Intell Syst Technol. 2011; 2:1–27.
12. Xu Y, Fish M, Gerlach J, et al. Combined quantitative analysis of attenuation corrected and non-corrected myocardial perfusion SPECT: Method development and clinical validation. J Nucl Cardiol. 2010; 17:591–599. [PubMed: 20387137]
13. Diamond GA, Forrester JS. Analysis of probability as an aid in the clinical diagnosis of coronary-artery disease. N Engl J Med. 1979; 300:1350–1358. [PubMed: 440357]
14. Karimi-Ashtiani S, Arsanjani R, Fish M, et al. Direct quantification of left ventricular motion and thickening changes using rest-stress myocardial perfusion SPECT. J Nucl Med. 2012; 53:1392–1400. [PubMed: 22872739]
15. Slomka PJ, Fish MB, Lorenzo S, et al. Simplified normal limits and automated quantitative assessment for attenuation-corrected myocardial perfusion SPECT. J Nucl Cardiol. 2006; 13:642–651. [PubMed: 16945744]
16. Germano G, Berman DS. On the accuracy and reproducibility of quantitative gated myocardial perfusion SPECT. J Nucl Med. 1999; 40:810–813. [PubMed: 10319755]
17. Nishina H, Slomka PJ, Abidov A, et al. Combined supine and prone quantitative myocardial perfusion SPECT: method development and clinical validation in patients with no known coronary artery disease. J Nucl Med. 2006; 47:51–58. [PubMed: 16391187]
18. Germano G, Kavanagh PB, Waechter P, et al. A new algorithm for the quantitation of myocardial perfusion SPECT. I: technical principles and reproducibility. J Nucl Med. 2000; 41:712–719. [PubMed: 10768574]
19. Sharir T, Germano G, Waechter PB, et al. A new algorithm for the quantitation of myocardial perfusion SPECT. II: validation and diagnostic yield. J Nucl Med. 2000; 41:720–727. [PubMed: 10768575]
20. Germano G, Kiat H, Kavanagh PB, et al. Automatic quantification of ejection fraction from gated myocardial perfusion SPECT. J Nucl Med. 1995; 36:2138–2147. [PubMed: 7472611]
21. Committee Members, Klocke FJ, Baird MG, Lorell BH, et al. ACC/AHA/ASNC Guidelines for the Clinical Use of Cardiac Radionuclide Imaging—Executive Summary. Circulation. 2003; 108:1404–1418. [PubMed: 12975245]
22. Germano G, Kavanagh PB, Slomka PJ, et al. Quantitation in gated perfusion SPECT imaging: the Cedars-Sinai approach. J Nucl Cardiol. 2007; 14:433–454. [PubMed: 17679052]

23. Slomka PJ, Berman DS, Xu Y, et al. Fully automated wall motion and thickening scoring system for myocardial perfusion SPECT: Method development and validation in large population. J Nucl Cardiol. 2012; 19:291–302. [PubMed: 22278774]
24. Wolak A, Slomka PJ, Fish MB, et al. Quantitative myocardial-perfusion SPECT: comparison of three state-of-the-art software packages. J Nucl Cardiol. 2008; 15:27–34. [PubMed: 18242477]
25. Chang C-C, Lin C-J. Training nu-support vector regression: theory and algorithms. Neural Comput. 2002; 14:1959–1977. [PubMed: 12180409]
26. Opper M, Urbanczik R. Universal learning curves of support vector machines. Phys Rev Lett. 2001; 86:4410–4413. [PubMed: 11328187]
27. Chung KM, Kao WC, Sun CL, et al. Radius margin bounds for support vector machines with the RBF kernel. Neural Comput. 2003; 15:2643–2681. [PubMed: 14577857]
28. DeLong ER, DeLong DM, Clarke-Pearson DL. Comparing the areas under two or more correlated receiver operating characteristic curves: a nonparametric approach. Biometrics. 1988; 44:837–845. [PubMed: 3203132]
29. Candelieri A, Conforti D. A hyper-solution framework for SVM classification: Application for predicting destabilizations in chronic heart failure patients. Open Med Inform J. 2010; 4:136–140. [PubMed: 21589851]
30. Mohebbi M, Ghassemian H, Asl BM. Structures of the recurrence plot of heart rate variability signal as a tool for predicting the onset of paroxysmal atrial fibrillation. J Med Signals Sens. 2011 May; 1(2):113–121. [PubMed: 22606666]
31. Berman DS, Kang X, Van Train KF, et al. Comparative prognostic value of automatic quantitative analysis versus semiquantitative visual analysis of exercise myocardial perfusion single-photon emission computed tomography. J Am Coll Cardiol. 1998; 32:1987–1995. [PubMed: 9857883]
32. Leslie WD, Tully SA, Yogendran MS, et al. Prognostic value of automated quantification of 99mTc-sestamibi myocardial perfusion imaging. J Nucl Med. 2005; 46:204–211. [PubMed: 15695777]
33. Emmett L, Iwanochko RM, Freeman MR, et al. Reversible regional wall motion abnormalities on exercise technetium-99m-gated cardiac single photon emission computed tomography predict high-grade angiographic stenoses. J Am Coll Cardiol. 2002; 39:991–998. [PubMed: 11897441]
34. Berman DS, Kang X, Gransar H, et al. Quantitative assessment of myocardial perfusion abnormality on SPECT myocardial perfusion imaging is more reproducible than expert visual analysis. J Nucl Cardiol. 2009; 16:45–53. [PubMed: 19152128]
35. Golub RJ, Ahlberg AW, McClellan JR, et al. Interpretive reproducibility of stress Tc-99m sestamibi tomographic myocardial perfusion imaging. J Nucl Cardiol. 1999; 6:257–269. [PubMed: 10385181]
36. Golub RJ, McClellan JR, Herman SD, et al. Effectiveness of nuclear cardiology training guidelines: a comparison of trainees with experienced readers. J Nucl Cardiol. 1996; 3:114–118. [PubMed: 8799236]
37. Holly TA, Abbott BG, Al-Mallah M, et al. Single photon-emission computed tomography. J Nucl Cardiol. 2010; 17:941–973. [PubMed: 20552312]

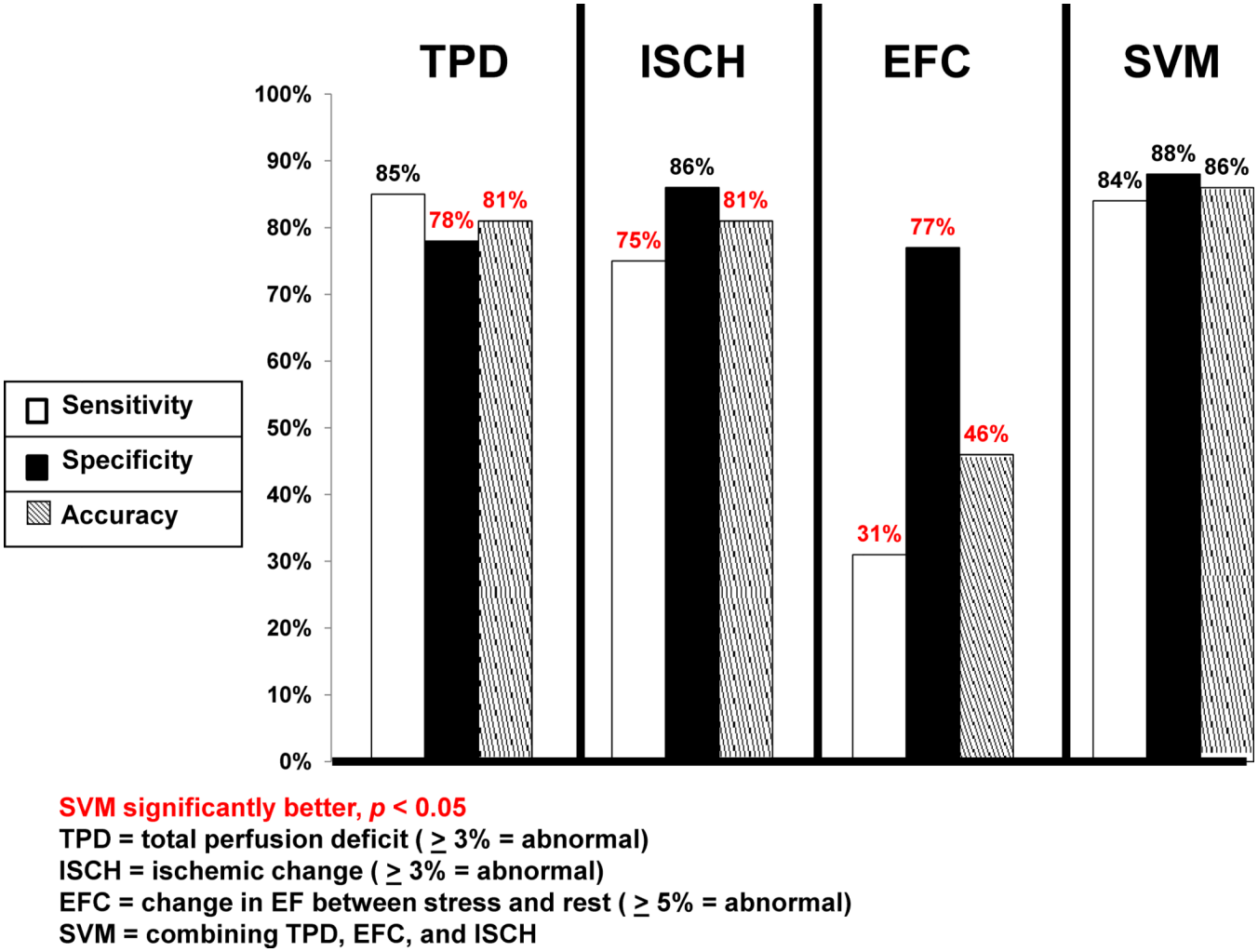

Figure 1.

Sensitivity, specificity and accuracy of Support Vector Machines (SVM) versus Total Perfusion Deficit (TPD), Ischemic Change (ISCH), and Ejection Fraction Change (EFC) for detection of ≥70% coronary artery lesions. Red indicates significant difference compared to SVM ($p < 0.05$).

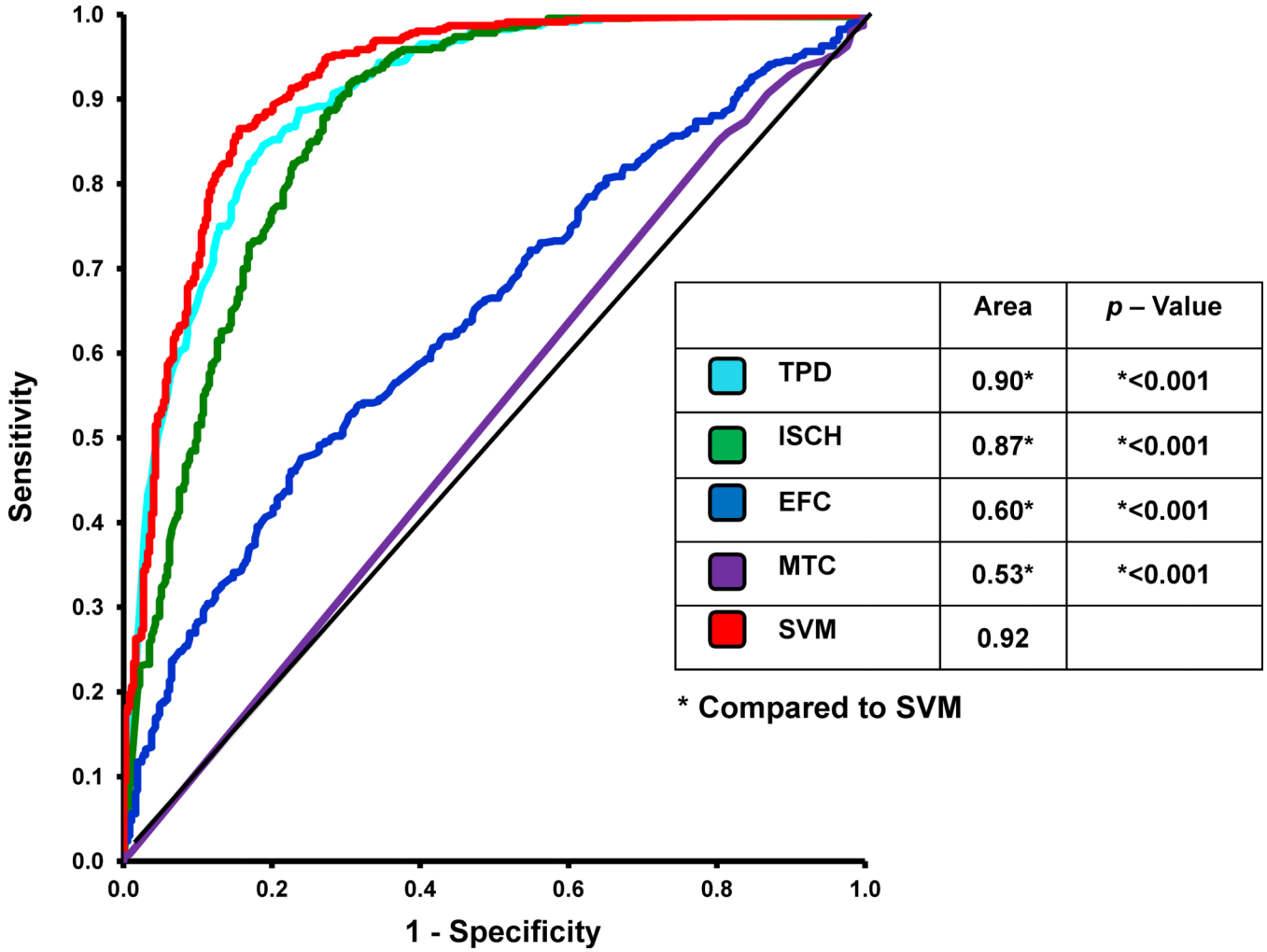

Figure 2.

The Receiver Operating Characteristic (ROC) curves comparing the Support Vector Machines (SVM) and Total Perfusion Deficit (TPD), Ischemic Change (ISCH), Motion and Thickening Change (MTC), and Ejection Fraction Change (EFC) for detection of ≥70% coronary artery lesions. * Indicates statistically significant difference compared to a SVM ($p < 0.05$).

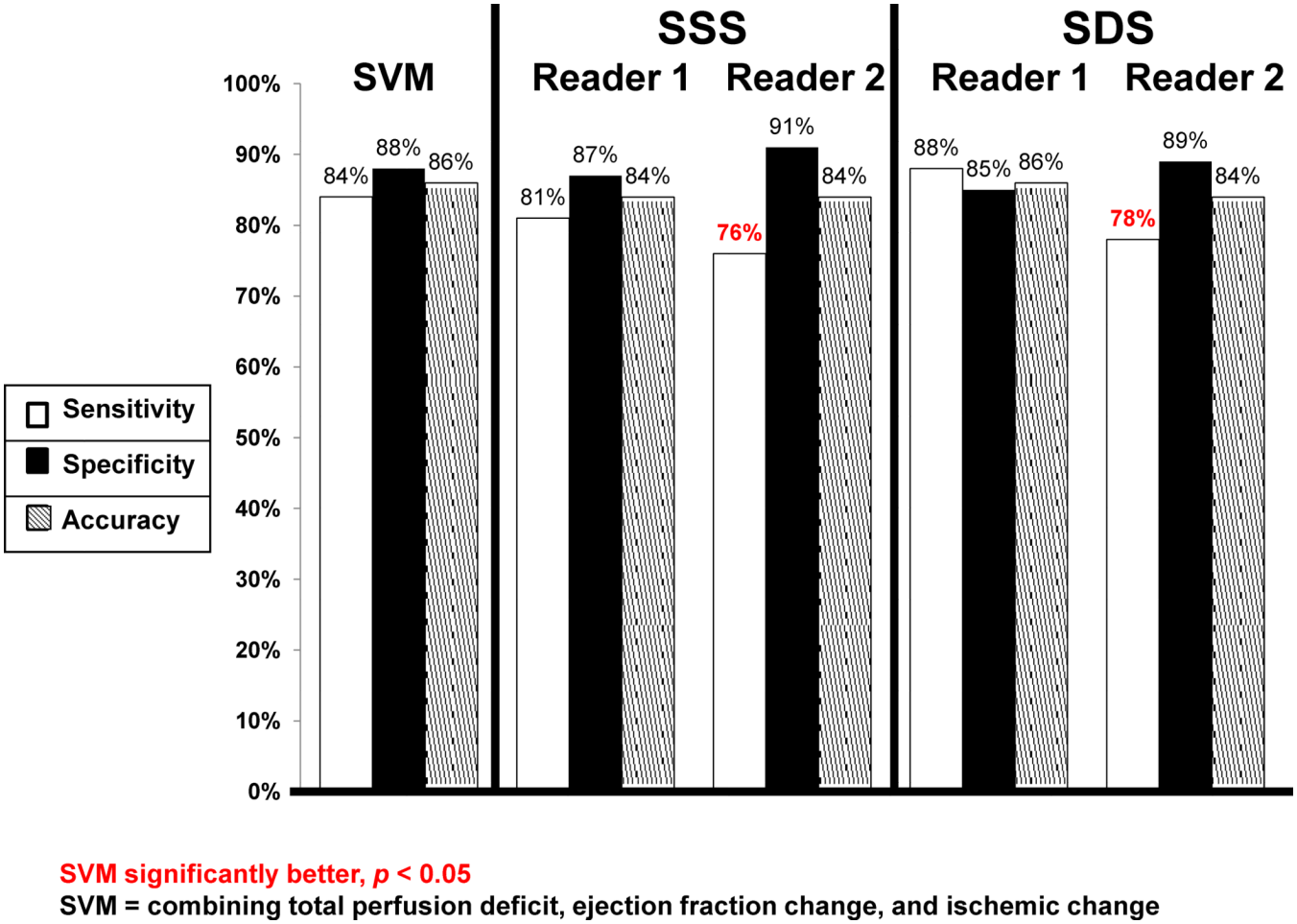

Figure 3.
Sensitivity, specificity and accuracy of Support Vector Machines (SVM) versus visual analysis (SSS and SDS) for detection of ≥70% coronary artery lesions. * Indicates statistically significant difference compared to SVM ($p < 0.05$).

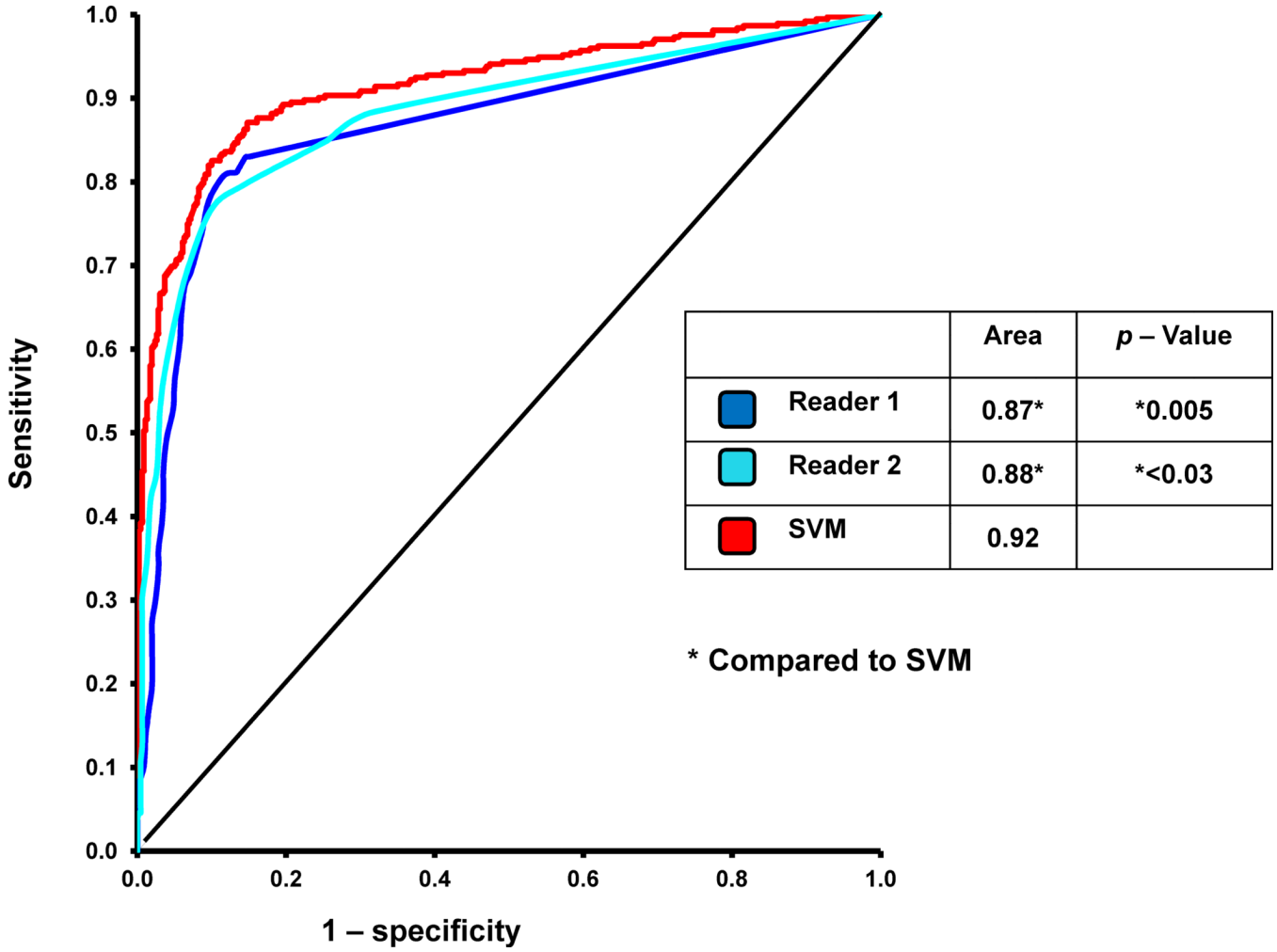

Figure 4.

The Receiver Operating Characteristic (ROC) curves comparing the Support Vector Machines (SVM) and visual analysis for detection of ≥70% coronary artery lesions. * Indicates statistically significant difference compared to SVM ($p < 0.05$).

TABLE 1

Baseline characteristics of the patients

	Train	Test	*p* – value
Number	125	832	N/A
Age (years)	60 ± 12	60 ± 12	NS
Male %	50%	50%	NS
Diabetes Mellitus %	18%	18%	NS
Hypertension %	57%	55%	NS
Hyperlipidemia %	44%	47%	NS
Smoking %	19%	20%	NS
LLk	25	309	N/A
0 – Vessel CAD	25	151	N/A
1 – Vessel CAD	25	172	N/A
2 – Vessel CAD	25	116	N/A
3 – Vessel CAD	25	84	N/A

N/A = Not Applicable, NS = Not Significant, LLk = Low-likelihood, CAD = Coronary Artery Disease

TABLE 2

Number of times the diagnosis was correctly changed when using SVM versus TPD

	N	ISCH	EFC	Both
Correctly identified as positive	10	10 (5.0% ± 1.1)	6 (−5.5% ± 3.1)	6 (pos)
Correctly identified as negative	53	49 (1.4% ± 1.5)	48 (1.5% ± 5.7)	44 (neg)

N = number, ISCH = ischemic change, EFC = ejection fraction change, pos = positive cases, neg = negative cases. Average values and standard deviations for the quantitative parameters are provided within the parenthesis.

TABLE 3

Comparison of SVM combining quantitative perfusion with different functional parameters

	SVM: TPD + ISCH + EFC	SVM: TPD + ISCH + MTC	SVM: TPD + ISCH + Volumes
Sensitivity	84%	77% *	74% *
Specificity	88%	93% *	94% *
Accuracy	86%	86%	85%
ROC-AUC	0.92	0.91	0.92

* Significantly different than SVM combining TPD, ISCH, and EFC, $P < 0.05$. TPD = Total perfusion deficit, ISCH = ischemic change, EFC = ejection fraction change, MTC = Motion and thickening change.